Original article

# Three-terraced evaporated ramp model for differentiation of the massive dolomitization process: Insights from the Lower Cambrian Longwangmiao Formation in the Sichuan Basin

Xin Jin[1], Jinmin Song[1]*, Shugen Liu[1], Zhiwu Li[1], Di Yang[1], Han Wang[1,2]

[1]*State Key Laboratory of Oil and Gas Reservoir Geology and Exploitation, Chengdu University of Technology, Chengdu 610059, P. R. China*

[2]*Department of Earth Sciences, University of Leeds, Leeds LS2 9JT, UK*

**Abstract:**
Within carbonate strata across the globe, dolostone reservoirs hold paramount importance in the realm of petroleum development. The genesis of dolostone has long perplexed geologists; however, despite the proliferation of various dolomitization models, the origin of dolostone and its capacity to elucidate the extensive dolomitization processes of the Lower Paleozoic on a platform scale remain subjects to debate. The present study endeavors scrutinizing the dolomitization process of the Lower Cambrian Longwangmiao Formation, with a particular emphasis on the impact of paleogeomorphology on platform- or basin-scale dolomitization. Through meticulous field observations, petrological examinations and geochemical analyses, the correlation between the distribution of dolostones and paleogeomorphological features is elucidated, thereby establishing a dolomitization model that considers paleogeomorphological features. In contrast to prior investigations, this study discerns that the dolomitization process of the Longwangmiao Formation is not only governed by depositional facies environments and sea-level fluctuations but also markedly influenced by paleogeomorphological factors. Specifically, a distinct compositional and distributional gradient of dolomite is observed from the higher terrace to the lower terrace. These findings not only provide novel insights into the dolomitization process within the Sichuan Basin but also serve as a useful reference for analogous processes at the basin or craton scale in other sedimentary basins. The proposed three-terraced evaporated seepage reflux dolomitization model offers a fresh vantage point for describing the extensive dolomitization processes of the Lower Paleozoic on a global platform scale, and underscores the pivotal role of paleogeomorphology in the dolomitization process.

## 1. Introduction

Dolostone reservoirs within carbonate strata play a crucial role in petroleum development worldwide (Warren, 2000). It is generally believed that dolomite is more resistant to compaction and dissolution than greywacke, and the dolomite reservoir space can be better preserved in ultra-deep strata (Li et al., 2024). Despite the fact that various dolomitization models have been proposed, the origin of dolostone and its ability to explain the massive dolomitization process of the Lower Paleozoic on a platform scale continue to puzzle geologists (Roberts, 2024). Currently, regarding the issue of large-scale dolomitization, it is widely accepted that seawater, as the primary magnesium ion reservoir, can provide abundant magnesium ions for the formation of large-scale dolomite (Machel, 2004). Typically, discussions surrounding

such dolomitization models put more emphasis on depositional facies environments and sea-level fluctuations (Liang et al., 2022; Jiang et al., 2023a). At the same time, the influence of paleogeomorphology on platform- or basin-scale dolomitization remains less explored.

During the Early Cambrian, dolostones were widely developed on a global scale, including the Xiaoerbulake and Shayilike Formations (Tarim Basin) (Wei et al., 2021; Zhang et al., 2023), the Longwangmiao Formation and Xixiangchi Group (Sichuan Basin) (Zhao et al., 2024), the Ara Group (Oman Basin) (Grotzinger and Al-Rawahi, 2014), and the Hawker Group (Officer Basin) (Kovalevych et al., 2006). The dolomitization of these strata is related to a strong evaporative environment. The thick layered dolostones of the Longwangmiao Formation form the primary oil and gas reservoirs in the Sichuan Basin (Li et al., 2021; Yang et al., 2024). Significant research has been conducted on the sequence stratigraphy, paleogeography and reservoir characteristics of this unit (Du et al., 2016; Li et al., 2023; Zhao et al., 2024). However, the key question in the exploration of this unit dolomite debate regards the genesis of dolomitization. Two dolomitization processes have been proposed so far. One describes a single stage of the dolomitization process, such as dolomitization by normal sea water in the Central Sichuan Basin (Zhou et al., 2015) or seepage reflux dolomitization in the Central and Eastern Sichuan Basin (Jiang et al., 2023b; Yang et al., 2024). The other proposed mechanism is a multi-stage dolomitization model involving seepage-reflux dolomitization, burial dolomitization and hydrothermal dolomitization (Liu et al., 2021a; Jiang et al., 2023a; Li et al., 2024). Apparently, previous studies on the dolomitization of the Longwangmiao Formation are mainly focused on analyzing the properties of multi-stage dolomitizing fluids. However, the paleogeomorphology of the Longwangmiao Formation in the Sichuan Basin, which is 'higher in the west and lower in the east', and the differential distribution of dolomites provide a possibility to further explore the relationship between the distribution of dolostones and paleogeomorphology.

On the above basis, this study selected the research objects as outcrops and boreholes with different degrees of dolomitization in different regions of the Sichuan Basin. Through detailed field observations, petrological and geochemical analysis, the principal aims were to:

1) Understand the mechanisms driving dolomitizing fluids;
2) investigate the genetic mechanisms of dolomitization in the Longwangmiao Formation;
3) establish a dolomitization model for the Longwangmiao Formation that considers paleogeomorphology.

The findings are expected to provide insights into dolomitization processes in other sedimentary basins at the basin or craton scale.

## 2. Geological setting

The Sichuan Basin, located in Southwestern China, is an intracratonic sedimentary basin in the upper Yangtze Block (Fig. 1(a)) (Liu et al., 2021c). Subsequent to the Ediacaran, the upper Yangtze Block underwent a complex sequence of tectonism ranging from extension to convergence (Han et al., 2024), forming a paleo-high along its western margin (Xu et al., 2016; Gu et al., 2023) and causing northeastern erosion of the Longwangmiao Formation in the basin's west (Zhou et al., 2015). During the Longwangmiao Formation deposition, the Sichuan Basin hosted an eastwardly inclined carbonate ramp (Du et al., 2016), with tidal flat, inner ramp, mid-ramp, outer ramp, and basin facies developing eastward in a thickness ranging from 90 to 300 m (Fig. 1(b)) (Du et al., 2016).

The Longwangmiao Formation exhibits terraced paleogeomorphology (Fig. 1(c)). The Central Sichuan Basin, near the western ancient land, has higher paleogeomorphological features and is affected by terrigenous rocks, forming grain shoals and inter-shoal sea deposits in the inner ramp environment (Xu et al., 2016; Gu et al., 2023; Zhao et al., 2024). The South Sichuan Basin, influenced by the Qiyueshan and Huayingshan faults (Fig. 1(a)), has medium paleogeomorphological features, forming "two highs and one depression" and the "Wanzhou-Yibin" Sag (Xu et al., 2016). Remarkably, up to 140 m of evaporites were deposited in the "Wanzhou-Yibin" Sag (Xu et al., 2016; Wang et al., 2023). In the Eastern Sichuan Basin on the east side of the Qiyueshan fault, grain shoals are extensively deposited, with partially dolomitized limestone and limestone appearing and transitioning eastward to mid-ramp facies.

## 3. Sampling and methods

This study collected samples from 10 boreholes and 3 outcrops in the Sichuan Basin (Fig. 1). Thin sections were prepared and analyzed optically using a Nikon Eclipse E600 POL. After this step, 74 samples ($< 120$ μm crystal size) were chosen, while later cement fillings were excluded. Powder samples ($< 200$ mesh) were prepared from duplicates using an agate mortar for carbon, oxygen and strontium isotope analysis as well as major and trace element analysis. Thirty-eight samples were selected for quantitative powder X-ray diffractometry. To compare the geochemical characteristics of partially dolomitized limestone, samples were taken from the Central, Southern and Eastern Sichuan Basin and tested for dolomicrites (*in-situ* DM), dolomitized grains (*in-situ* DG), and calcite cements (*in-situ* CC). This process yielded forty-four *in-situ* trace element data points and thirty-three carbon, oxygen and strontium isotope data points (see Appendix for detailed test locations, Fig. S1). Twenty-two dolostone, four mudstone and eight partially dolomitized limestone samples were selected for calcium isotope analysis. For details, see the Appendix.

## 4. Results

### 4.1 Lithology

#### 4.1.1 Dolostone

(1) Fabric-retentive dolomitic textures

Dolomudstones (DM) are mostly composed of micritic dolomite (Fig. 2(a)), with a horizontal distribution that is typically uniform and thin-layered. They exhibit a dull luminescence under cathodoluminescence (CL) microscopy (Figs.
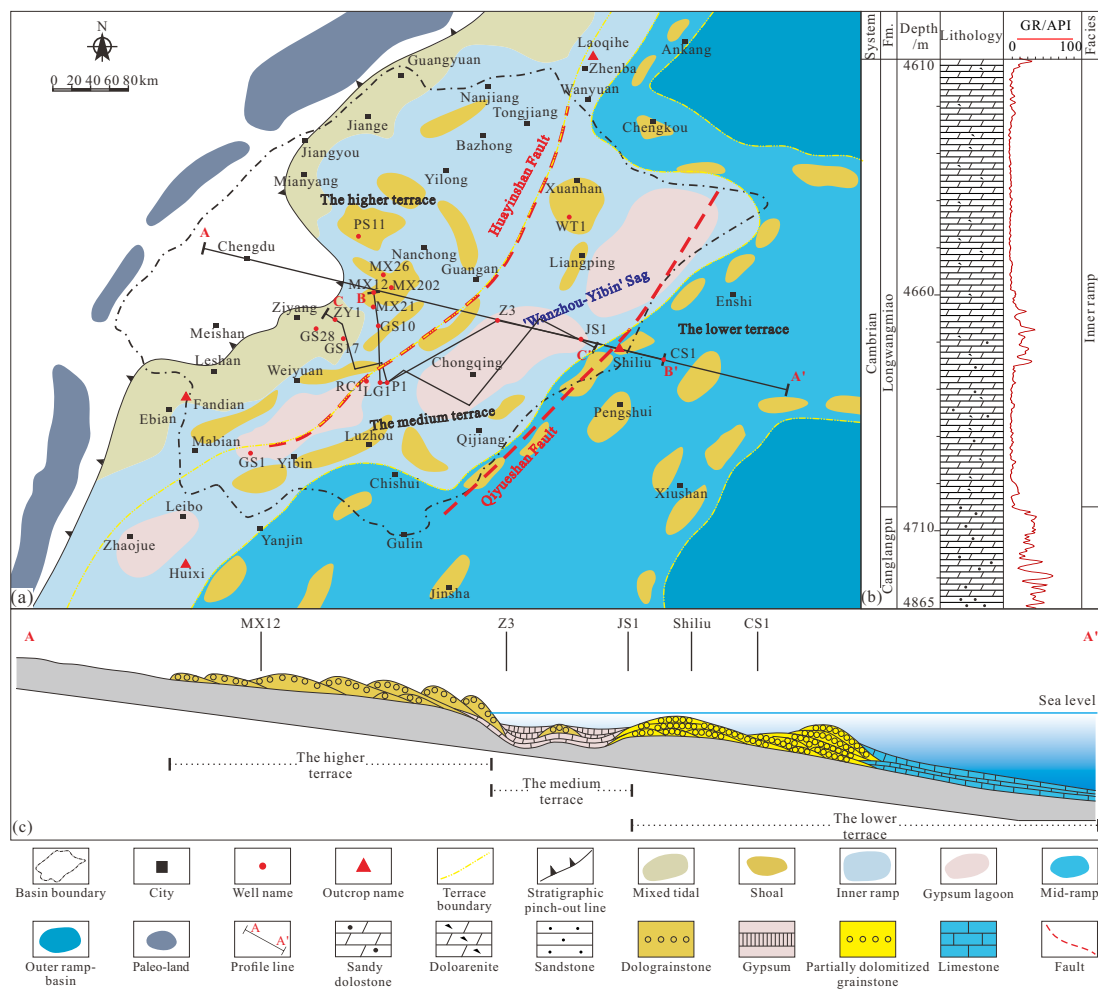
**Fig. 1**. (a) Sedimentary facies of the Longwangmiao Formation (modified after Du et al. (2016)); (b) lithostratigraphic columns in the GS10 well and (c) sedimentary model of the Longwangmiao Formation (Location AA', modified from Du et al. (2016)).

2(b)-2(c)). Due to the influence of the western paleocontinent, approximately 2% of DM contain terrigenous clastics (Fig.2(d)). These siliciclastics are mostly composed of well-sorted, rounded, silt-grained sand ranging from 0.01 to 0.03 mm. Additionally, gypsum is frequently present in mud-crystalline dolomites, with its content typically ranging from 1% to 10% (Fig. 2(e)). To differentiate these two distinct types of DM, we hereinafter refer to them as silty dolostone and gypsum-containing dolostone. DM are common in the Longwangmiao Formation, comprising about 25% of all dolostones studied.

Dolograinstones (DG) are originally present as granular and oolitic rocks (Figs. 2(f)-2(g)), with grain content ranging from 60% to 80%. The cortices and nuclei of oolites are constituted by planar-s and non-planar-a silty to fine crystals, measuring 5 to 20 μm in size, whereas the cements predominantly consist of planar-e and planar-s fine crystals, ranging from 20 to 100 μm. Under CL microscopy, the remnant grains or ooids, with dimensions spanning from 0.2 to 1 mm, exhibit dull red luminescence, while the cements exhibit bright red luminescence (Fig. 2(g)). DG are prevalent in the Longwangmiao Formation, comprising approximately 35% of

the studied dolostones.

(2) Fabric-obliterated dolomitic textures

Fine crystalline dolostones (CD) have a relatively low content (approximately 20%) and consist of planar-e to planar-s fine crystals (crystal sizes of 50-120 μm; Figs. 2(h)-2(k)). No sedimentary or structural features are present in this dolomite stage. Under CL, CD exhibit bright red luminescence with uniform characteristics (Fig. 2(k)).

### 4.1.2 Partially dolomitized limestone

Dolomitic grainstones and dolomitic limestones are dark grey, thin-bedded and exhibit a patchy appearance, with dark patches as dolostone and light patches as limestone (Fig. 2(l)). The dolomite content ranges from 30% to 50%. Relic ooidal and intraclastic textures can be observed, ranging in size from silt to gravel. The dolomite crystals are mostly between 25 and 30 μm, while the calcite spar crystallines are silt-sized and partially replaced by dolomite.

Calcareous dolograinstones and calcareous dolostones are dark grey, medium-bedded and display dolomitization within ooid and intraclast ghosts at the microscopic level (Fig. 2(m)). Their dolomite content ranges from 50% to 85%, with crystal
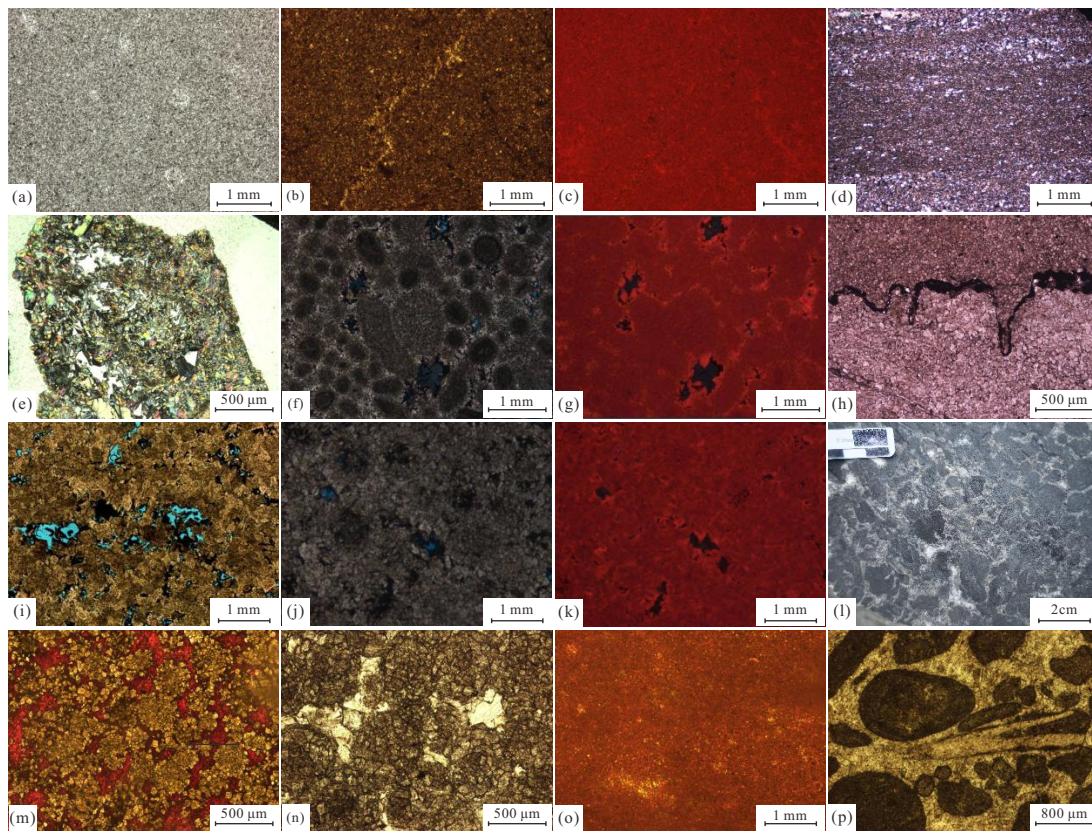
**Fig. 2**. Lithology of the Longwangmiao Formation. (a) Dolomudstone, MX202, 4683.22 m, plane polarized light (PPL); (b) dolomudstone, Huixi outcrop, PPL; (c) CL image of (b), dull red luminescence; (d) Silty dolostone, MX202, 4,734.84 m, cross polarized light (CPL); (e) gypseous dolostone, GS1, 3,898 m, CPL; (f) dolograinstone, MX26, 4,916.11 m, PPL; (g) CL of (g), where relic grains are represented by dull red luminescence and cements by bright red luminescence; (h) crystalline dolostone, irregular stylolites, MX21, 4,600.86 m, PPL; (i) crystalline dolostone, MX202, 4,675.37 m, PPL; (j) crystalline dolostone, MX26, 4,927.33 m, PPL; (k) CL image of (k), dull red luminescence; (l) dark grey rudstone of dolomitic limestone with an intraclastic size of 0.4 ~ 1.5 cm, Laoqihe outcrop; (m) residual calcareous dolograinstone, with a grain-supported fabric, Laoqihe outcrop, PPL; (n) residual calcareous dolograinstone, with a grain-supported fabric, LG1, 4,834.54 m, PPL; (o) mudstone, Laoqihe outcrop, PPL and (p) grainstone, with a grain-supported fabric, Laoqihe outcrop, PPL.

sizes of 25-30 μm.

Weakly dolomitic grainstones, weakly dolomitic limestones, weakly calcareous dolograinstones, and weakly calcareous dolostones are dark grey and medium-bedded. The dolomite or calcite content is usually less than 15%. Microscopically, the dolomite crystals range from 5-30 μm, while the calcite crystals range from 2-30 μm. Weakly dolomitic grainstones and weakly calcareous dolograinstones retain residual ooid and intraclast ghosts textures (Fig. 2(n)).

### 4.1.3 Limestone

Mudstones (MS) are dark grey, non-granular or thin-bedded, with particle sizes under 10 μm and a calcite content exceeding 85% (Fig. 2(o)).

Grainstones consist of spherical to ellipsoidal intraclasts, ranging from 0.3 to 1.8 mm in size, with grain content exceeding 60% (Fig. 2(p)). The grains are primarily sand-sized, rounded or oval, with silt-sized or fine crystalline calcite cement filling the intergranular dissolution pores.

## 4.2 Composition and properties

### 4.2.1 Major and trace elements

A total of 118 analyses were conducted for major and trace elements by targeting MgO, CaO, Mn, Fe, Sr, and Na (Table S1). The results showed that in the Central Sichuan Basin, the contents of MgO and CaO are similar in DM, DG and CD, with slightly lower MgO in *in-situ* DM. Na content is highest in DG and DM, moderate in CD and lowest in *in-situ* DMs. Fe content is highest in CD, followed by DGs and DM, and lowest in *in-situ* DM. Al content is highest in DG, followed by CD, DM and *in-situ* DM. Mn content is highest in CD, followed by DG, DM and *in-situ* DM. Sr levels are highest in DG, followed by CD, DM and *in-situ* DM. In the Southern Sichuan Basin, MgO content is significantly lower in *in-situ* CC, while DM, DG, CD, and *in-situ* DG have similar levels. CaO content is highest in *in-situ* CC, with lower levels in others. Na content is highest in DMs, followed by DG, CD, *in-situ* DG, and lowest in *in-situ* CC. Fe content is highest in DM, followed by CD, DG, *in-situ* DG, and lowest in *in-situ*

CC. Al content is highest in CD, followed by DM, with DG being intermediate, and *in-situ* DG and CC being the lowest. Mn content is highest in DG, followed by CD and DM, with *in-situ* DG showing intermediate levels and *in-situ* CC being the lowest. Sr content is highest in *in-situ* CC, followed by DM and CD, with *in-situ* DG showing intermediate levels and DG being the lowest. In the Eastern Sichuan Basin, MgO content is highest in DM, DG and CD, intermediate in *in-situ* DG, and lowest in *in-situ* CC and MS. CaO content is highest in *in-situ* CC and MS, and is lower in others. Na content is highest in DM, followed by DG, CD, *in-situ* DG, MS, and *in-situ* CC. Fe content is highest in DG, followed by DM, CD, *in-situ* DG, MS, and lowest in *in-situ* CC. Al content is highest in DM, followed by CD, DG, *in-situ* DG, and lowest in *in-situ* CC and MS. Mn content is highest in CD, followed by DG, DM, *in-situ* DG, MS, and *in-situ* CC. Sr content is highest in MS, followed by *in-situ* CC, intermediate in DM, DG and CD, and lowest in *in-situ* DG.

### 4.2.2 Rare-earth elements (REE) and order degree of dolostone crystals

In the Central Sichuan Basin, the average total REE ($\Sigma$REE) contents of DM and DG are the highest, significantly exceeding those in the Southern and Eastern Sichuan Basin. The average $\Sigma$REE content of CD exhibits a decreasing trend from the Central to the Eastern Sichuan Basin. The average $\Sigma$REE content of *in-situ* DM in the Central Sichuan Basin is significantly higher than that of *in-situ* DG in the Southern and Eastern Sichuan Basin. Meanwhile, the average $\Sigma$REE content of *in-situ* CC in the Southern Sichuan Basin is slightly higher than that in the Eastern Sichuan Basin, and the average $\Sigma$REE content of MS is comparable to that of *in-situ* CC in both the Southern and the Eastern Sichuan Basin (Table S1). CD consistently exhibit the highest degree of crystalline order, followed by DG with moderate values and DM with the lowest levels (Table S2).

### 4.2.3 Carbon, oxygen and strontium isotope

In the Central Sichuan Basin, DG exhibit the lowest $\delta^{13}$C values, whereas *in-situ* DMs exhibit the highest $\delta^{13}$C values. The $\delta^{13}$C values of DM and CD are intermediate and closely match those of *in-situ* DMs. Regarding the $\delta^{18}$O values, DGs exhibit the lowest values, while DM have the highest, while CD and *in-situ* DM show intermediate values. In terms of $^{87}$Sr/$^{86}$Sr ratios, DM exhibit low ratios, whereas DG and CD exhibit wider and higher ranges. *In-situ* DM show higher $^{87}$Sr/$^{86}$Sr ratios (Table S3). In the Southern Sichuan Basin, DM exhibit the lowest $\delta^{13}$C values, while *in-situ* CC show the highest. DG exhibit the second highest $\delta^{13}$C values, while CD and *in-situ* DG display intermediate values. For $\delta^{18}$O values, *in-situ* DG exhibit the lowest values, while DG have the highest, and those in DM, CD and *in-situ* CC are intermediate. In terms of $^{87}$Sr/$^{86}$Sr ratios, DM exhibits the highest and most stable ratios; DG and CD display intermediate ratios, while *in-situ* DG show ratios similar to CD, and *in-situ* CC have the lowest ratios (Table S3). In the Eastern Sichuan Basin, DM exhibit the highest $\delta^{13}$C values, while *in-situ* CC show the lowest. *In-situ* DG, MS, CD, and DG display intermediate

$\delta^{13}$C values. For $\delta^{18}$O values, DG exhibit the lowest values, while DM shows the highest, with *in-situ* CC, MS, CD, and *in-situ* DG displaying intermediate values. In terms of $^{87}$Sr/$^{86}$Sr ratios, DM exhibit a wide range, while DG display a wider and higher range, and CD and *in-situ* DG exhibit relatively narrower ranges. *In-situ* CC and MS show the lowest $^{87}$Sr/$^{86}$Sr ratios (Table S3).

### 4.2.4 Calcium isotopes

The $\delta^{44}$Ca values in the Central and Southern Sichuan Basin exhibit consistent ranges. Conversely, $\delta^{44}$Ca values in the Eastern Sichuan Basin are notably more negative compared to those in the Central and Southern Sichuan Basins. The $\delta^{44}$Ca values of partially dolomitized limestone in the Eastern Sichuan Basin overlap with those of the dolostones in the Central and Southern Sichuan Basin, although they are less negative than those of the dolostones in the Eastern Sichuan Basin. Among all samples, limestone exhibits the least negative $\delta^{44}$Ca values (Table S4).

## 5. Interpretation and discussion

### 5.1 Three geomorphological terraces exist on the ramp

The higher terrace covering the Central Sichuan Basin is located along Mabian, Weiyuan, Guang'an, and Yilong to Nanjiang. The strata thickness is 70 to 100 m. It is dominated by silty dolostone (Fig. S2a) and DG in lithology and the evaporated mixed tidal flat (Figs. S2a-S2b), storm tidal flat (Fig. S2c), and inner ramp grain bank eastward in the microfacies (Fig. S3a) (Du et al., 2016; Song et al., 2021). The medium terrace constitutes a series of grabens, such as Yibin, Chongqing, Wanzhou, and Bazhong, which are related to the syn-sedimentary faults in both margins in thickness of 150 to 300 m. The medium terrace is represented by the Southern Sichuan Basin, within which the gypsum, gypseous dolostone (Fig. 2(e)), argillaceous limestone, and limy dolostone settle down in the evaporated lagoon microfacies (Fig. S3a). However, the seaward lower terrace covering the lower terrace distributes along Chishui, Pengshui, and Enshi to Chengkou, with the total thickness ranging from 100 to 250 m. Limestone (Figs. S2f-S2g), argillaceous limestone and dolomitic limestone (Figs. S2d-S2e) are predominant in lithology, and periodical storms occur within the outer ramp facies (Fig. S2f) (Song et al., 2021). Moreover, the 2D seismic section through the boreholes of ZY1, GS17, P1 and JS1 also reveals an eastward thickening trend and seismic facies transition resulting from the three terraces (Fig. S3b). It measures about 20 to 30 ms in two-way time and presents as chaotic or irregular reflection structures for the ZY1-GS17-P1 area in the higher terrace, pointing to the grain bank microfacies within the inner ramp. However, the two-way time is up to 60 to 100 ms toward JS1 within the medium terrace and shortly continuous bedded reflection structures are dominant, leading to the restricted lagoon microfacies (Fig. S3b).

## 5.2 Diagenetic sequence and timing of dolomitization

The grain size of DMs, ranging from 10 to 50 μm (Fig. 2(a)), coupled with the preservation of fabric in DGs (Fig. 2(f)), implies that MS and DG could have been the antecedents of DM. This observation points towards the notion that dolomitization occurred under near-surface conditions at relatively low temperatures (Sibley and Gregg, 1987). While it is acknowledged that dolomite crystals exhibiting non-planar textures can potentially form at temperatures marginally above 50-60 °C (Gregg and Sibley, 1984), their precipitation at lower temperatures is also plausible, particularly in environments characterized by highly supersaturated fluids, with temperatures falling below the 50-60 °C threshold (Gregg and Sibley, 1984). Considering the presence of gypsum/anhydrite (Fig. 2(e)), DM and DG appear to have formed in a near-surface diagenetic environment (Preto et al., 2015). In contrast, the larger crystal size of CD, spanning from 50 to 120 μm (Figs. 2(h)-2(j)), along with their subhedral to euhedral morphologies, suggests a higher-temperature formation environment compared to that of DM and DG, which is corroborated by the brighter CL of CD (Fig. 2(k)). Furthermore, the presence of crosscutting stylolites (Fig. 2(h)), whose genesis necessitates a minimum burial depth of approximately 600 m (Fabricius and Borre, 2007), substantiates the assumption that CD formed within a shallow burial environment.

## 5.3 Composition and properties of the dolomitization fluids

### 5.3.1 Geochemical data validity assessment

Previous studies have demonstrated that dolostone geochemical data can be altered by diagenesis and terrigenous detrital input, making it challenging to directly reflect the original geological characteristics (Brand and Veizer, 1981; Derry et al., 1992; Qing and Veizer, 1994; Li et al., 2009). Herein, the diagenetic changes of samples from the Longwangmiao Formation were evaluated on the basis of the Mn/Sr ratio (Brand and Veizer, 1981) and $\delta^{18}O$ values (Li et al., 2009). It was found that the degrees of diagenetic changes in the lower, medium and higher terraces were slight, relatively slight and moderate, respectively, indicating that the existing data effectively retain the early diagenetic records. Concurrently, indicators such as the content of terrigenous-related element Al and the REE composition were used to evaluate the impact of detritus on the content of trace elements (Elbra et al., 2023). It was found that terrigenous materials have a greater impact on the concentrations of Na, Sr, Fe, Mn, and REE in dolomite samples in the higher platform, while this effect is relatively small on the medium and lower platforms. By removing samples with high Al contents, the influence of terrigenous materials was effectively mitigated, ensuring the accuracy of the analysis and the discussion of dolomitization-related fluid information (see Appendix and the supplemental assessment of diagenetic effects in the Supplementary material).

### 5.3.2 Dolomitization of Central Sichuan Basin within the higher terrace

For dolostone in the higher terrace, the contents of MgO and CaO were significantly negatively correlated (Fig. 3(a)), with an Mg/Ca ratio between 0.55 and 0.65, giving an average of 0.62 (Fig. 3(b)), and a larger order degree of dolomite from 0.61 to 0.83, giving an average of 0.71 (Fig. 3(c)).

The dolostones from the higher terrace are characterized by the highest concentration of Fe, Mn and Na and the lowest concentrations of Sr (Fig. 3) compared to those from the other two terraces. The average Na content of dolostones in the higher terrace is 660.46 ppm, significantly exceeding the values observed in the lower terrace, medium terrace and MS. This indicates that hypersaline brines, sourced from seawater evaporation, acted as the dolomitization fluids. According to the concentration variations of Fe, Mn and Sr, it can also be speculated that the dolomitization process within the higher terrace had the longest duration.

Trace elements such as Na, Sr, Fe, and Mn can reflect the sedimentary environment and the properties of the diagenetic fluids (Wang et al., 2021). During burial diagenesis, there is a general trend of decreasing Na and Sr content and increasing Fe and Mn content in dolostone, with the concentration of Na as an indicator of salinity (Wang et al., 2021). In this work, the original seawater information is considered to be recorded in the MS samples selected from the lower terrace.

It is worth mentioning that, compared to MS and DG, the higher terrace of CD shows the highest order degree and the highest Fe and Mn contents, while the Na and Sr contents are the lowest. The other two terraces only exhibit this pattern in terms of order degree and Na content. To investigate this further, the grain sizes of the same type of dolostone across the three terraces were analyzed. A consistent trend was found: The grain size of dolostone is always largest in the lower terrace, intermediate in the medium terrace and smallest in the higher terrace. Therefore, we believe that the higher terrace may preserve the more pristine trace element characteristics of different types of dolostone, while the loss of this pattern in the medium and lower terraces may be due to the enlargement of dolomite crystals.

The concentrations of REE in the dolostone result from the equilibrium between diagenetic fluids and carbonate rocks (Wang et al., 2014). In general, the influence of precipitated minerals on REE compositions is much smaller than that of the primary fluids such as seawater (Lottermoser, 1992). The concentrations of REE in chondrites typically exhibit lower values as those observed in Post-Archean Australian Shale (PAAS), Upper Continental Crust (UCC), and seawater. Within the trio of PAAS, UCC and seawater, the highest REE content have been consistently found for Ce, with chondrites displaying a Ce content that is only surpassed by Y, thereby manifesting a negative $\delta Ce$ value. However, utilizing these reference materials for normalization may, to a certain extent, obscure the discernible trends of light rare earth element (LREE) enrichment and heavy rare earth element (HREE) depletion within the samples under investigation. In fact, the genesis of dolomite diverges markedly from that of shale
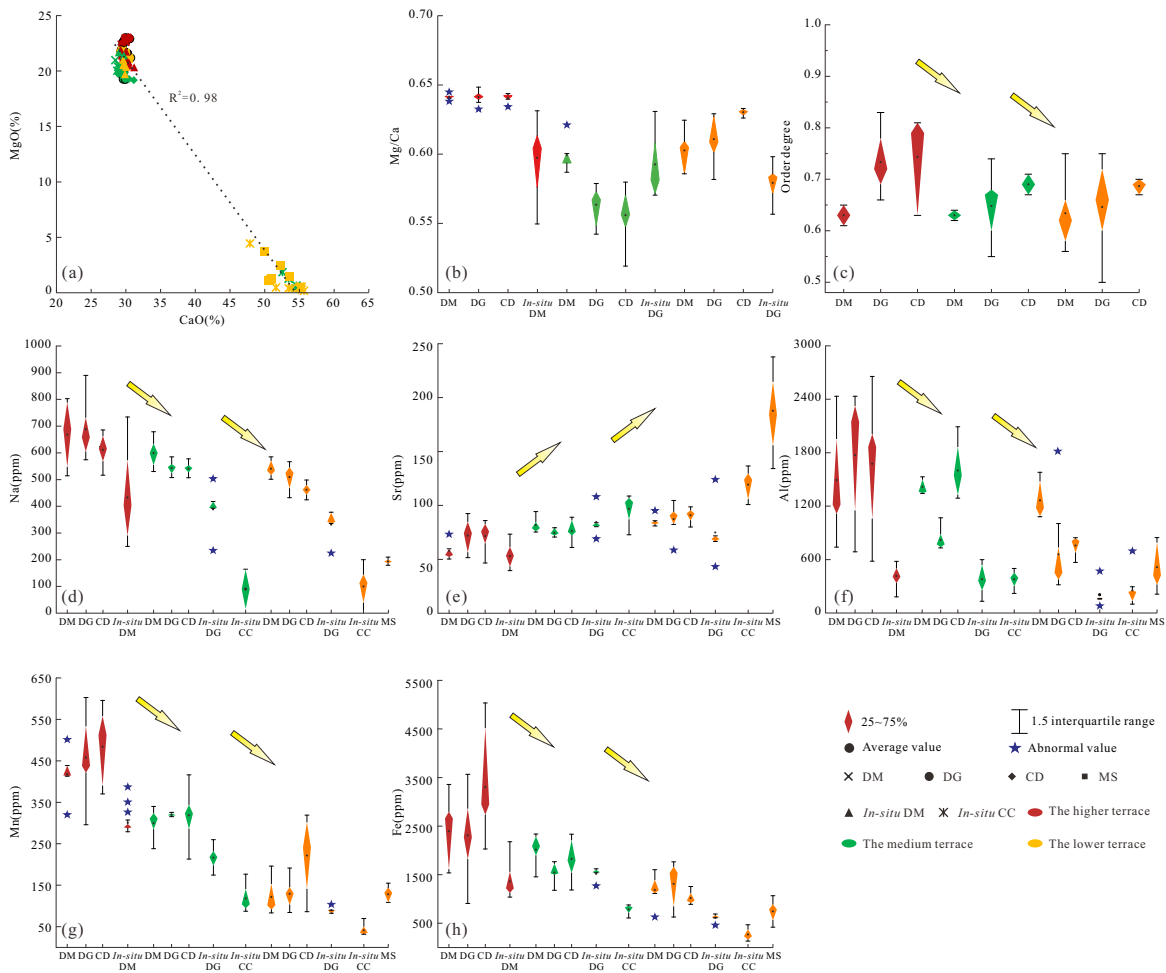
**Fig. 3**. MgO-CaO content, Mg/Ca ratios and trace elements of different lithologies. (a) Scatterplot of MgO-CaO content; (b) Mg/Ca ratio in different lithologies; (c) crystal order of different types of dolostones; (d) Na within different lithologies; (e) Sr in different lithologies; (f) Al in different lithologies; (g) Mn in different lithologies and (h) Fe in different lithologies.

and chondrites. While there is no intrinsic close correlation between the formation processes of these materials, dolomite formation is inextricably linked to the characteristics and composition of the dolomitizing fluids involved (Kawabe et al., 1998; Xiang et al., 2020). Actually, the REE patterns of seawater, especially the identification of diagenetic fluids, have been discussed in detail (Bau and Dulski, 1996; Wang et al., 2014; Li et al., 2023). The ΣREE of all samples in the higher terrace was less than 20 ppm, with an average of 5.82 ppm, indicative of the typical lower REE abundance in marine carbonates (Qing and Mountjoy, 1994). The (La/Yb)n ratios were greater than 1.97, demonstrating the enrichment of LREE. In addition, the $\delta$Ce of dolostones in the higher terrace showed positive anomalies, similar to the characteristics of marine carbonates (Fig. 4) (Hu et al., 2010). However, no positive $\delta$Eu anomalies occurred in the higher terrace, suggesting the absence of hydrothermal input.

The $\delta^{13}$C and $\delta^{18}$O values of dolostones are mainly influenced by the primary depositional fabrics as well as the salinity and temperature of the diagenetic fluids (He et al., 2014). During the early Cambrian Longwangmiao Formation period, the $\delta^{13}$C and $\delta^{18}$O of seawater ranged from

-2.5‰ to 1.9‰ and -9.8‰ to -7‰, respectively (Veizer et al., 1999) (Fig. 5(a)). The $\delta^{18}$O of dolostone is generally more positive than those of early Cambrian seawater, though some DG samples exhibit $\delta^{18}$O values within the seawater range. Furthermore, the $\delta^{13}$C values of dolostone from the higher terrace align closely with those of seawater. These dolostones occupy a higher position in the Mn/Sr versus $\delta^{18}$O scatterplots, showing an ascending trend from DG to DM and then to CD, indicative of strong dolomitization (Fig. 5(b)). In contrast to MS within the lower terrace, $\delta^{18}$O is slightly more positive and $\delta^{13}$C remains relatively unchanged in the dolostones, indicating that the dolomitization fluids within the higher terrace are seawater-sourced in an evaporative, possibly hypersaline environment (Wang et al., 2021) (Figs. 5(a)-5(b)).

It has been argued that the larger $^{87}$Sr/$^{86}$Sr ratios during the Cambrian era are related to the Pan-African-Brazilian orogeny phase (Denison et al., 1998). As such, a large amount of crust-derived strontium transferred into the seawater during the Longwangmiao Formation period due to the tectonic uplift of the upper Yangtze block in the Pan-African phase (Veizer et al., 1999). The $^{87}$Sr/$^{86}$Sr ratios of dolostone at the higher terrace were found to be significantly larger than those

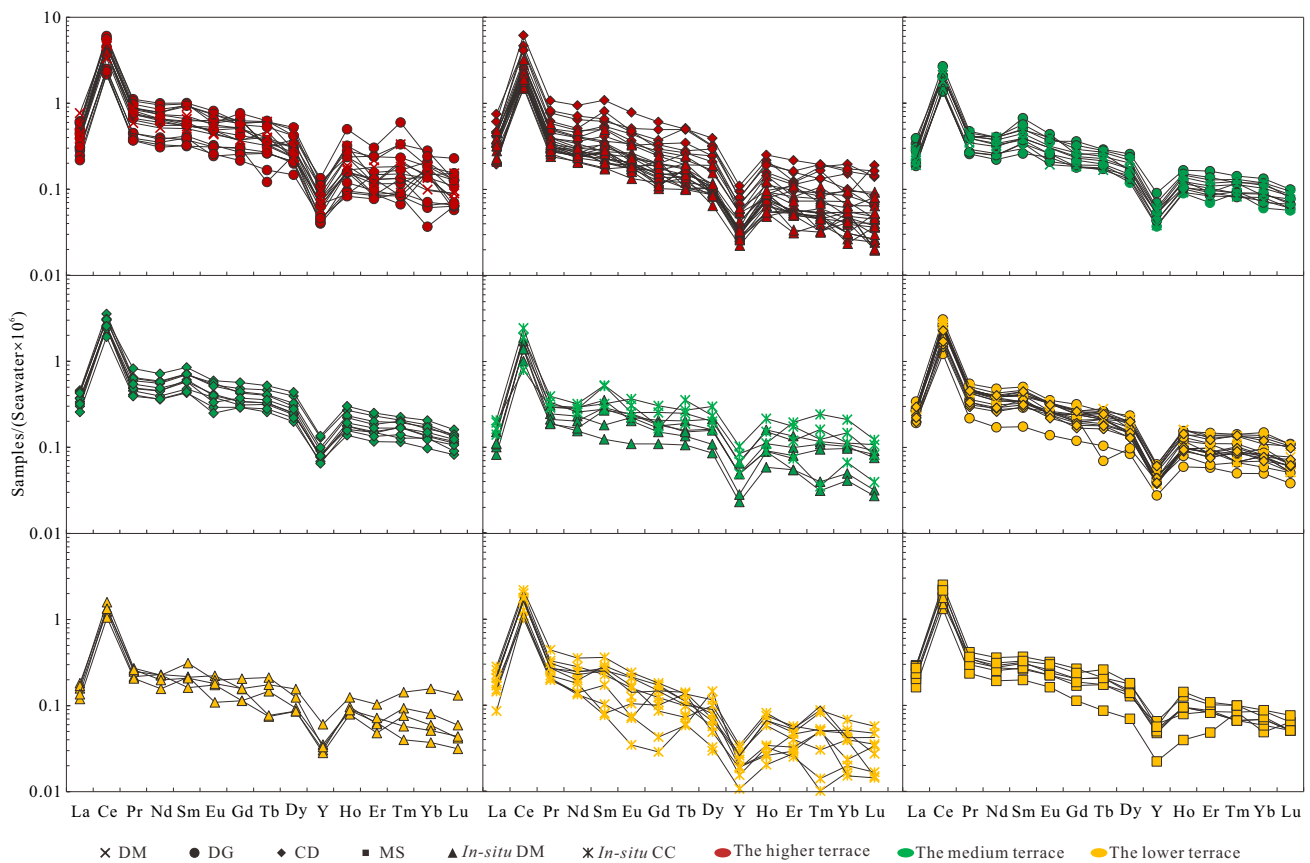**Fig. 4**. REE distribution pattern of dolostones.

of seawater (Fig. 5(c)). Compared with the $^{87}Sr/^{86}Sr$ ratio range of 0.708693 to 0.709135 in MS, those of dolostones at the higher terrace exhibit the largest positive numerical difference, with a descending trend from CD, DG to DM in the scatterplots of $^{87}Sr/^{86}Sr$-$\delta^{18}O$ (Figs. 5(c)-5(d)). However, it is more likely that isotope 87Sr is discharged from the brines during dolomitization, resulting in an increase in the $^{87}Sr/^{86}Sr$ ratio and reflecting the differentiation in the extent of dolomitization. Therefore, it is speculated from the $^{87}Sr/^{86}Sr$ results that the diagenetic fluids at the higher terrace are seawater-sourced brines.

Recently, a calcium isotope has been applied to interpret the seawater-related dolomitization process occurring in both the early diagenesis by the fluid-buffered model and the later alteration by the sediment-buffered model (Ahm et al., 2018; Higgins et al., 2018; Wei et al., 2022). The early-stage dolomitization process has significantly altered the $\delta^{44}Ca$ of shallow marine carbonates, as reported for the modern Bahama carbonate platform, showing a positive trend under seawater-buffered conditions and negative variation by the sediment-buffered model (Ahm et al., 2018; Higgins et al., 2018). Dolostones in the higher terrace have relatively higher $\delta^{44}Ca$, which is similar to modern Bahama dolostones (Higgins et al., 2018). Considering the models of $\delta^{44}Ca$ fractionation in the Ediacaran to Cambrian of the South China craton (Wei et al., 2022), the $\delta^{44}Ca$ of dolostones at the higher terrace is typical for the fluid-buffered to the sediment-buffered transition

model (Figs. 5(e)-5(f)). In the scatterplots of $\delta^{13}C$ and $\delta^{44}Ca$, the dolostone in the higher terrace is similar to MS of the lower terrace, which is thought to be related to the original aragonite precursor during the process of neometamorphism (Wei et al., 2022). Thus, the $\delta^{44}Ca$ ratios within the higher terrace can provide clues to the contemporaneous seawater composition (Fig. 5(g)), suggesting the influence of seawater-sourced dolomitized fluids.

### 5.3.3 Dolomitization of the Southern Sichuan Basin within the medium terrace

For dolostone in the medium terrace, there is a negative correlation between the MgO and CaO contents (Fig. 3(a)): Mg/Ca ratios are between 0.52 and 0.63, giving an average of 0.57, and the order degree of dolomite is in a medium value from 0.44 to 0.84, giving an average of 0.65, which all lead to the products of early-stage dolomitization (Fig. 3(c)).

Dolostones of the medium terrace have moderate contents of certain elements such as Fe, Mn, Na, and Sr (Fig. 3). The average Na content in dolostones of the medium terrace is 554.71 ppm (Fig. 3(d)), which is much higher than that of MS but remains moderate compared to the other two terraces. In addition, laser *in-situ* trace element analyses show that the Na characteristics of the dolomitized grains are similar to those of the whole-rock samples. Together, these features indicate that the salinity of the dolomitized fluids is lower than that in the higher terrace. Based on the concentrations of Fe, Mn
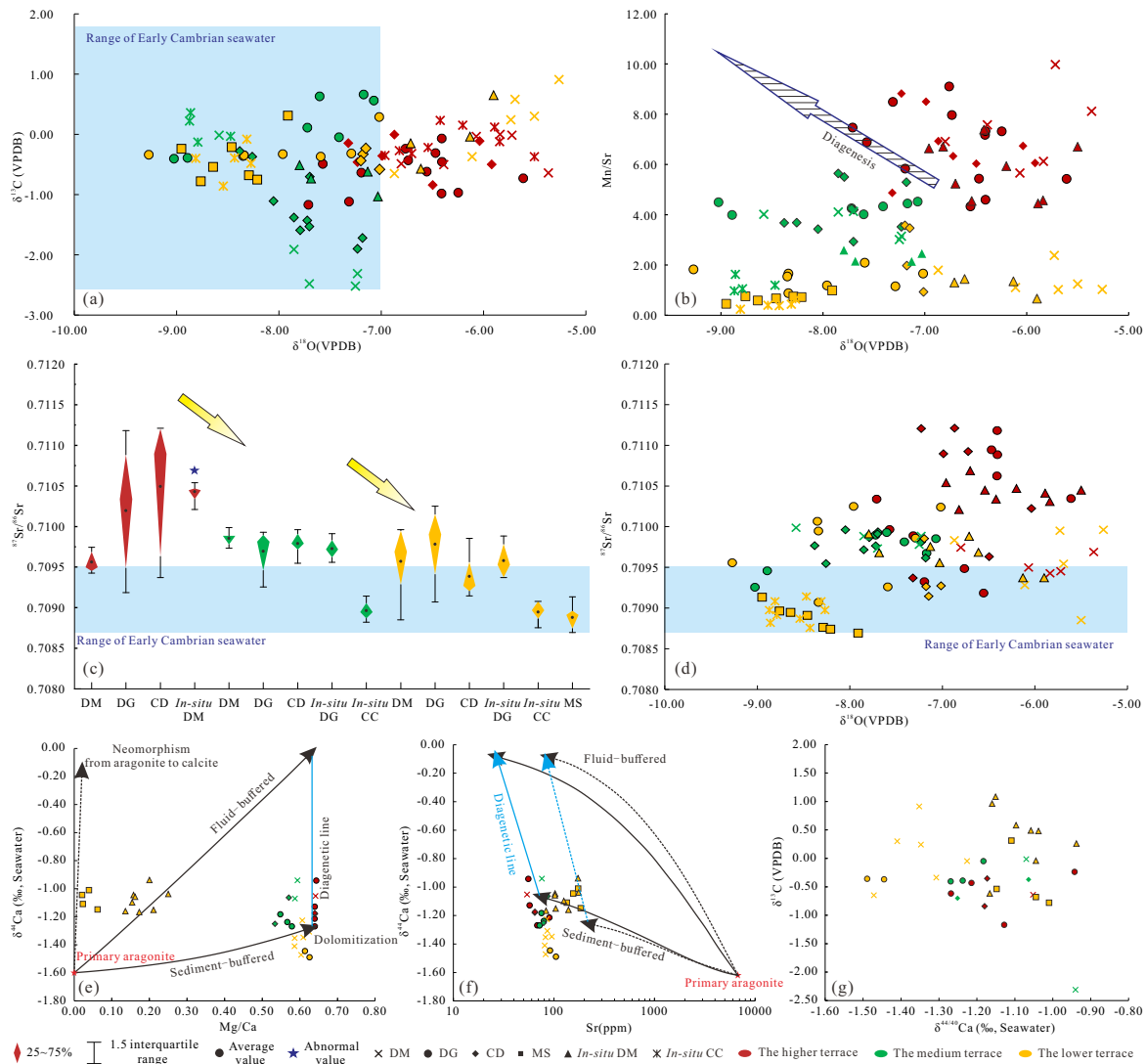
**Fig. 5**. (a) Scatterplots of $\delta^{13}C$-$\delta^{18}O$, (b) Mn/Sr-$\delta^{18}O$, (c) box plot of $^{87}Sr/^{86}Sr$ ratios, (d) scatterplots of $^{87}Sr/^{86}Sr$-$\delta^{18}O$, (e) $\delta^{44}Ca$-Mg/Ca ratio, (f) $\delta^{44}Ca$-Sr content and (g) $\delta^{44}Ca$-$\delta^{13}C$ value. In the context of plot (e) and (f), these data are complemented by the application of a shallow-marine diagenetic model (Ahm et al., 2018). In the context of plot (f), solid lines delineate the trajectories associated with the marine dolomitization of primary aragonite, while dashed lines illustrate the neomorphic transformation from primary aragonite to the extant calcite. The black arrows within the figure panels signify the degree of alteration experienced by the bulk sediment, ranging from 0% to 100% and following the direction indicated by the arrows, under the influence of various diagenetic pathways. The blue lines demarcate the compositional variability range, which is bounded by a fully diagenetic mineral that transitions from a fluid-buffered endmember to a sediment-buffered endmember.

and Sr, it is believed that the dolomitization process within the medium terrace occurred over a moderate diagenetic duration. The LREE-enriched pattern is also present in dolostones within the medium terrace, as indicated by (La/Yb)n ratios greater than 1.06. The positive $\delta$Ce anomalies in dolostones, without corresponding positive $\delta$Eu anomalies, match the characteristics of typical marine carbonate sediments (Fig. 4).

The $\delta^{18}O$ and $\delta^{13}C$ values of dolostones in the medium terrace are mostly within the range of early Cambrian seawater (Fig. 5(a)). This differs from those in the higher and lower terraces, where $\delta^{18}O$ and $\delta^{13}C$ values are significantly more positive compared to seawater (Fig. 5(a)). However, the $\delta^{18}O$ values of dolostones are still positive in the medium ter-

race compared to MS, suggesting an evaporative environment (Wang et al., 2021). The negative $\delta^{13}C$ values of DM and CD may result from continued burial coupling during the Early Cambrian (Derry et al., 1994). *In-situ* laser $\delta^{18}O$ and $\delta^{13}C$ analyses showed that *in-situ* CC has a similar signature to MS, while *in-situ* DG has significantly positive $\delta^{18}O$ and $\delta^{13}C$ values, similar to DG. In contrast, the slightly positive $\delta^{13}C$ values of DG and the more negative $\delta^{13}C$ values of DM and CD compared to MS may reveal the early dolomitization of DG, followed by the shallow burial dolomitization of DM and CD. The dolostones of the medium terrace are mostly located in the middle range, with an ascending trend from CD to DM to DG in the scatterplots of Mn/Sr ratio and

$\delta^{18}$O, demonstrating that the moderate level of dolomitization resulted from seawater-sourced brines (Fig. 5(b)).

The $^{87}$Sr/$^{86}$Sr ratios of dolostone are generally higher than those of early Cambrian seawater (Fig. 5(c)), with an increasing trend from *in-situ* CC, *in-situ* DG, DG, and CD to DM in terms of the averaged value. In contrast to the MS and *in-situ* CC, dolostones at the medium terrace are slightly more positive in both $^{87}$Sr/$^{86}$Sr and $\delta^{18}$O (Fig. 5(d)), with a moderate numerical gap, indicating an incomplete dolomitization process by seawater-sourced brines, particularly in grainstones. Furthermore, there is a gradually decreasing trend in the $^{87}$Sr/$^{86}$Sr ratio of dolostones from the higher to the medium terrace (Fig. 5(c)), which may be related to the consumption of seawater-sourced brines and the progression of the shallow burial dolomitization process in the medium terrace.

Dolostones in the medium terrace have higher $\delta^{44}$Ca and lower Sr content, similar to those in the higher terrace and the modern Bahamian bank (Higgins et al., 2018). In the scatterplots of $\delta^{13}$C and $\delta^{44}$Ca, dolostones in the medium terrace also display a typical transition fractionation model of $\delta^{44}$Ca from fluid-buffered to sediment-buffered conditions (Figs. 5(e)-5(f)). Compared to dolostones of the higher terrace and MS from the lower terrace, dolostones in the medium terrace have slightly more positive $\delta^{13}$C and much more negative $\delta^{44}$Ca, which indicates a sedimentary buffering trend related to the mineralogical transformation during the dolomitization process in the shallow burial environment (Wei et al., 2022).

### 5.3.4 Dolomitization of the Eastern Sichuan Basin within the lower terrace

For dolostones of the lower terrace, there is a negative correlation between MgO and CaO contents (Fig. 3), with Mg/Ca ratios ranging from 0.58 to 0.63, giving an average of 0.6. The order degree of the dolomite is the lowest among all three terraces, ranging from 0.5 to 0.75, giving an average of 0.62. This indicates incomplete dolomitization in the early stage (Fig. 3(c)).

In the lower terrace, dolostones have the lowest content of Fe and Mn and the highest Sr concentrations, similar to MS (Fig. 3). The average Na content, measured at 509.15 ppm (Fig. 3(c)), is larger than MS but the lowest among the three terraces. Furthermore, laser *in-situ* trace element analyses revealed significantly lower Na, Mn, Sr, and Fe contents in calcite cement compared to dolomites. Therefore, it is assumed that the dolomitization process in the lower terrace was driven by seawater-sourced brines with the lowest salinity over the shortest duration.

The analyses show that the average of (La/Yb)$_n$ ratio is 2.91, indicating an LREE-enriched pattern. Positive $\delta$Ce anomalies are apparent but positive $\delta$Eu anomalies are absent in dolostones (Fig. 4), similar to the characteristic of marine limestones (Hu et al., 2010). The $\delta^{18}$O and $\delta^{13}$C values of DG and CD in the lower terrace are mostly within the early Cambrian seawater range, while those of DM and *in-situ* DG are slightly more positive (Fig. 5(a)). The $\delta^{18}$O values of dolostones are also slightly more positive, showing an increasing trend from DG, CD to DM, in contrast to the MS,

indicating an evaporative environment (Wang et al., 2021). The $\delta^{13}$C values of DM are much more positive than those of MS, indicating the early-stage dolomitization of grainstone followed by the shallow burial dolomitization of MS (Fig. 5(a)). In the scatterplots of Mn/Sr ratio and $\delta^{18}$O, this is mostly located in the lowest position for the dolostones of the lower terrace, showing an ascending trend from MS, DG, CD to DM, which demonstrates the smallest dolomitization extent by evaporated seawater-sourced brines (Fig. 5(b)).

The $^{87}$Sr/$^{86}$Sr ratios of DG and DM are mostly higher than the early Cambrian seawater range, while those of CD and MS fall within this range (Fig. 5(c)). There is an ascending trend in the averaged value from MS, *in-situ* CC, *in-situ* DG, CD, and DG to DM (Fig. 5(c)). Compared to MS, dolostones at the lower terrace have slightly more positive values in both $^{87}$Sr/$^{86}$Sr and $\delta^{18}$O (Fig. 5(d)), albeit with the smallest numerical difference. This indicates an incomplete dolomitization process by seawater-sourced brines, prioritizing grainstone in the burial diagenetic environment. Furthermore, a decreasing trend in the $^{87}$Sr/$^{86}$Sr ratio of dolostones from the medium to lower terrace has been observed (Fig. 5(c)), which may be related to the deficiency of seawater-sourced brines and the partially shallow burial dolomitization process in the lower terrace.

The typical sediment-buffered model of calcium isotopes dominates in dolostones within the lower terrace, while the fluid-buffered model occurs in dolomitic limestones or limy dolostones (Figs. 5(e)-5(f)). The completely fluid-buffered end is present within the limestones in the scatterplots of $\delta^{13}$C and $\delta^{44}$Ca (Fig. 5(f)). Therefore, it is believed that seawater information is recorded in MS at the sediment-buffered end. Partially dolomitized limestones, such as dolomitic limestones or limy dolostones, show more affinity to MS. However, due to the significant differences in $\delta^{44}$Ca and $\delta^{13}$C, dolomitization fluids in the lower terrace are mostly distinct from the local seawater (Fig. 5(g)). This is likely related to the eastwardly migrated evaporated brines, as speculated from the similarity of dolostones in both the lower and the higher terraces.

### 5.4 Dolomitization Process for the entire Sichuan Basin

The dolomitization of the Longwangmiao Formation in the Sichuan Basin occurred on a three-terraced evaporated ramp, as indicated by the lithology, paleogeography and dolomitization differentiation. The higher terrace is represented by the Central Sichuan Basin, which is adjacent to paleo-land to the northwest. It is dominated by silty dolostones and DG, with depositional microfacies such as mixed tidal flats, storm tidal flats, and grain banks appearing eastwardly within the higher terrace (Figs. S2a-S2c). A strongly evaporative environment, driven by sea level fall and westward uplift, dominates this terrace. Thus, the contemporaneous dolomitization, driven by intense evaporation pumping, influenced both the grainstones and the mudstones (Figs. 6(a)-6(b)). The dolostones within the higher terrace are mostly composed of micritic to silt-sized crystalline dolomites with recognizable original grain fabrics or ghosts as a result of rapid dolomitization in the contem-
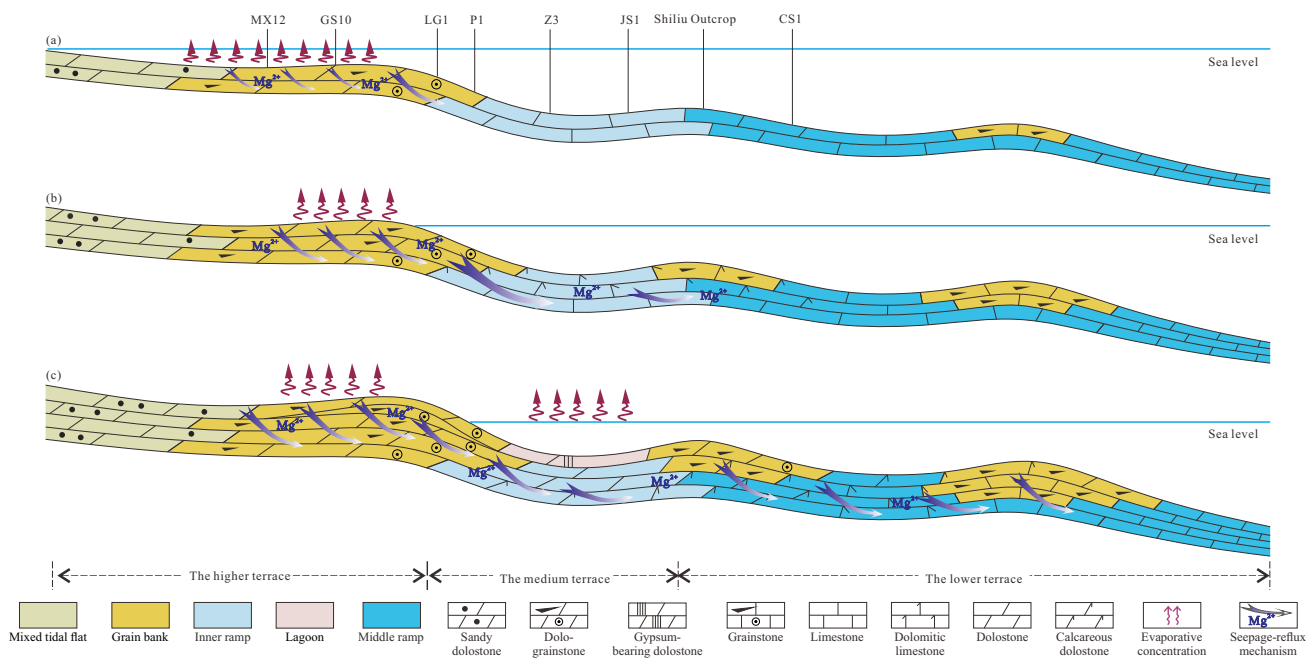
**Fig. 6**. Dolomitization model of the Longwangmiao Formation.

poraneous to penecontemporaneous phase. The dolomitization fluids are thought to be the most hypersaline brines sourced from seawater. In addition, the dolomitization process persisted over time, maintained by a periodic balance of tidal or storm currents and evaporation.

The medium terrace encompasses the Southern Sichuan Basin, which is moderately elevated in topography and located next to the Central Sichuan Basin to the west. In terms of lithology, it is mostly composed of gypsum, gypseous dolostone, dolograinstone, argillaceous limestone, and calcareous dolostone. The evaporated lagoon microfacies are widespread within the medium terrace, barred by the intraplatform grain bank constructions to the east (Figs. 6(b)-6(c)). The medium terrace is covered by restricted to evaporated lagoons in the grabens, related to the syn-sedimentary faults on both margins during the Longwangmiao Formation regression phase. The penecontemporaneous dolomitization process of seepage-reflux occurs in both the grainstones and the mudstones (Fig. 6(b)). The dolostones here are mostly composed of micritic to silt-sized crystalline dolomites with grain ghosts, resulting from rapid dolomitization in the penecontemporaneous phase. The dolomitization fluids are thought to be brines sourced from seawater with moderate salinity. The duration of dolomitization is moderate, influenced by shallow burial brines.

The lower terrace includes the Eastern Sichuan Basin, which is topographically at the lowest elevation, close to the Southern Sichuan Basin to the west and the open sea to the east. In the Longwangmiao Formation, dolostones, partially dolomitized limestones (Figs. S2d-S2e) and mudstones (Figs. S2f-S2g) coexist. The mid-ramp depositional facies dominate within the lower terrace, with some patchy grain bank microfacies developing. The shallow burial dolomitization process first takes place in the grainstones and then in the mudstones (Fig. 6(c)). The dolostones mostly comprise silt-sized crystalline

dolomites, resulting from incomplete dolomitization in the shallow burial phase. The dolomitization fluids are related to brines sourced from seawater with the lowest salinity. Under the influence of the shallow burial brines, the dolomitization duration here is the shortest.

In the Lower Cambrian Longwangmiao Formation in the Sichuan Basin, the three-terraced eastwardly inclined ramp controls the massive dolomitization process. The evaporation intensity shows a descending trend from the higher terrace to the medium terrace and toward the lower terrace. Research indicates that the evaporated hypersaline dolomitization fluids sourced from seawater also follow a concentration gradient, resulting in total dolomitization in the Central Sichuan Basin, the highest dolomitization in the Southern Sichuan Basin, and partial dolomitization in the Eastern Sichuan Basin. Therefore, in this paper, a three-terraced evaporated dolomitization system is proposed, driven by seawater-sourced brines migrating eastward from the higher to lower terrace, driven by topography, density, gravity and concentration gradients. The dolomitization processes are mostly contemporaneous evaporation pumping in the higher terrace, seepage-reflux in the penecontemporaneous phase in the medium terrace, and shallow burial dolomitization in the lower terrace. This three-terraced evaporated seepage reflux dolomitization model helps to enhance our understanding of the massive worldwide dolomitization process of the lower Paleozoic on a platform scale.

## 5.5 Implications

Scientists have proposed various models to explain the genesis of dolomites. Some of the most prominent models include dolomitization by normal seawater (Land, 1985), reflux seepage dolomitization (Land, 1985), mixing zone dolomitization (Badiozamani, 1973), Sabha dolomitization (Bush, 1973), hy-

drothermal dolomitization (Braithwaite and Rizzi, 1997), and burial dolomitization (Mattes and Mountjoy, 1980). However, mass balance calculations and reactive transport modeling have largely refuted the burial model and mixing zone dolomitization models, while hydrothermal dolomites are considered to be more localized (Machel, 2004). Despite the disparities in the hydrological and geochemical intricacies among these models, a consensus prevails among the majority of researchers that extensive dolomitization, particularly at the platform scale, necessitates the presence of a precursor carbonate substrate, an ample reservoir of magnesium ions ($Mg^{2+}$), and an efficacious mechanism for fluid transport (Land, 1985). To explain large-scale platform dolomitization, the seepage reflux model in evaporative environments is commonly used (Ryan et al., 2020). Prior studies have investigated the dolomitization mechanism of this model from two perspectives. From a geochemical perspective, in warm arid environments, the precipitation of evaporites reduces the calcium ion ($Ca^{2+}$) concentrations within the solution. This concomitantly elevates the Mg/Ca ratio, thereby inducing a state of oversaturation with respect to dolomite in the fluid (Patterson and Kinsman, 1982). From a hydrological perspective, evaporation provides the driving force for fluid flow, as the denser evaporating saline waters may infiltrate the underlying limestone (Machel, 2004).

Recent studies have revealed the potential key role of paleotopography in dolomitization in the Lower Paleozoic (Li et al., 2021). Unfortunately, most of these studies only discuss paleotopography in a general sense, without a systematic investigation of its specific impacts. In the Early Paleozoic, large-scale dolomite formations in evaporative environments have been reported in numerous basins worldwide, such as the Sichuan Basin (China) (Gu et al., 2019), Tarim Basin (China) (Liu et al., 2021b), Oman Salt Basin (Oman) (Grotzinger and Al-Rawahi, 2014), and Ordos Basin (China) (Fu et al., 2019). Warren (2010) compared the global sedimentation volume of evaporites with global plate-tectonic cycles and found that orogenic events, plate amalgamation and early continental rifting have all contributed to the formation of significant amounts of evaporites since the Phanerozoic. This is because tectonic activities during geological history often result in paleotopographical variations, creating restricted environments conducive to evaporite deposition, thus providing favorable conditions for large-scale dolomitization. This study provides a comprehensive explanation of paleotopography-controlled dolomitization in a large-scale evaporative environment, offering a new perspective for employing the permeation reflux model in evaporative environments. It is suggested that tectonic processes leading to a differential subsidence of carbonate platforms, influenced by paleotopography, in turn impact the paleotopography and subsequently influence the dolomitization process. This account of the correlation between the distribution of dolostones and paleogeomorphological features helps us unravel the mysteries of large-scale dolomitization in the Early Paleozoic.

## 6. Conclusions

In this paper, the correlation between the distribution of dolostones and paleogeomorphological features within the Sichuan Basin has been elucidated via field observations and *ex-situ* petrological and geochemical analyses. Seawater becomes increasingly restricted and hypersaline from the lower terrace to the middle and to the higher terrace. The hypersaline brines formed in the higher terrace triggered the process of extensive penecontemporaneous seepage reflux dolomitization, while residual brines flowed eastward to the middle and lower terraces, causing partial dolomitization. On the basis of these phenomena, a three-terraced evaporated seepage reflux dolomitization model has been proposed in this work, which significantly enhances our understanding of the massive global dolomitization process taking place in the Lower Paleozoic on a platform scale.

## Acknowledgements

## Supplementary file

https://doi.org/10.46690/ager.2025.03.05

## Conflict of interest

The authors declare no competing interest.

## References

Ahm, A. S. C., Bjerrum, C. J., Blättler, C. L., et al. Quantifying early marine diagenesis in shallow-water carbonate sediments. Geochimica et Cosmochimica Acta, 2018, 236: 140-159.

Badiozamani, K. The dorag dolomitization model, application to the middle Ordovician of Wisconsin. Journal of Sedimentary Petrology, 1973, 43: 965-984.

Bau, M., Dulski, P. Distribution of yttrium and rare-earth elements in the Penge and Kuruman iron-formations, Transvaal Supergroup, South Africa. Precambrian Research, 1996, 79(1-2): 37-55.

Braithwaite, C. J. R., Rizzi, G. The geometry and petrogenesis of hydrothermal dolomites at Navan, Ireland. Sedimentology, 1997, 44(3): 421-440.

Brand, U., Veizer, J. Chemical diagenesis of a multicomponent carbonate system; 2, stable isotopes. Journal of Sedimentary Research, 1981, 51(3): 987-997.

Bush, P. Some aspects of the diagenetic history of the sabkha in Abu Dhabi, Persian Gulf, in The Persian Gulf, Holocene Carbonate Sedimentation and Diagenesis in a Shallow Epicontinental Sea, edited by B. H. Purser, Springer, New York, pp. 395-407, 1973.

Denison, R. E., Koepnick, R. B., Burke, W. H., et al. Construction of the Cambrian and Ordovician seawater $^{87}$Sr/$^{86}$Sr curve. Chemical Geology, 1998, 152(3-4): 325-340.

Derry, L. A., Brasier, M. D., Corfield, R. M., et al. Sr and C isotopes in Lower Cambrian carbonates from the Siberian craton: A paleoenvironmental record during the 'Cambrian explosion'. Earth and Planetary Science Letters, 1994, 128(3-4): 671-681.

Derry, L. A., Kaufman, A. J., Jacobsen, S. B. Sedimentary cycling and environmental change in the Late Proterozoic: Evidence from stable and radiogenic isotopes. Geochimica et Cosmochimica Acta, 1992, 56(3): 1317-1329.

Du, J., Zhang, B., Wang, Z., et al. Sedimentary mode and reservoir genesis of dual grain banks at the Lower Cambrian Longwangmiao Fm carbonate ramp in the Sichuan Basin. Natural Gas Industry B, 2016, 3(5): 399-408.

Elbra, T., Soták, J., Kdýr, Š., et al. Cretaceous to Palaeogene boundary events and palaeoenvironmental responses across pelagic sequences of the Žilina core section, Slovakia: Rock magnetic, biotic, and geochemical characterization. Palaeogeography, Palaeoclimatology, Palaeoecology, 2023, 625: 111682.

Fabricius, I. L., Borre, M. K. Stylolites, porosity, depositional texture, and silicates in chalk facies sediments. Ontong Java Plateau-Gorm and Tyra fields, North Sea. Sedimentology, 2007, 54: 183-205.

Frimmel, H. E. Trace element distribution in Neoproterozoic carbonates as palaeoenvironmental indicator. Chemical Geology, 2009, 258: 338-353.

Fu, S., Zhang, C., Chen, H., et al. Characteristics, formation and evolution of pre-salt dolomite reservoirs in the fifth member of the Ordovician Majiagou Formation, mid-east Ordos Basin, NW China. Petroleum Exploration and Development, 2019, 46(6): 1153-1164.

Gregg, J. M., Sibley, D. F. Epigenetic dolomitization and the origin of xenotopic dolomite texture. Journal of Sedimentary Research, 1984, 54: 908-931.

Grotzinger, J., Al-Rawahi, Z. Depositional facies and platform architecture of microbialite-dominated carbonate reservoirs, Ediacaran-Cambrian Ara Group, Sultanate of Oman. AAPG Bulletin, 2014, 98(8): 1453-1494.

Gu, Z., He, Y., Peng, Y., et al. "Multiple-lagoon" sedimentary model of the Lower Cambrian gypsum-salt rocks in the Sichuan Basin. Acta Sedimentologica Sinica, 2019, 37(4): 834-846. (in Chinese)

Gu, Z., Jian, X., Watts, A. B., et al. Formation and evolution of an Early Cambrian foreland basin in the NW Yangtze Block, South China. Journal of the Geological Society, 2023, 180(3): jgs2022-2127.

Han, Y., Ran, B., Santosh, M., et al. The Cambrian collision of the Yangtze Block with Gondwana: Evidence from provenance analyses. GSA Bulletin, 2024, 137(1-2): 594-612.

He, X., Shou, J., Shen, A., et al. Geochemical characteristics and origin of dolomite: A case study from the middle assemblage of Ordovician Majiagou Formation Member 5 of the west of Jingbian Gas Field, Ordos Basin, North China. Petroleum Exploration and Development, 2014,

41(3): 417-427.

Higgins, J. A., Blättler, C. L., Lundstrom, E. A., et al. Mineralogy, early marine diagenesis, and the chemistry of shallow-water carbonate sediments. Geochimica et Cosmochimica Acta, 2018, 220: 512-534.

Hu, W., Chen, Q., Wang, X., et al. REE models for the discrimination of fluids in the formation and evolution of dolomite reservoirs. Oil & Gas Geology, 2010, 31(6): 810-818. (in Chinese)

Jiang, H., Liang, J., Azmy, K., et al. Controls of sedimentary facies and sealevel fluctuation on dolomitization: The Lower Cambrian Longwangmiao Formation in Sichuan Basin, China. Marine and Petroleum Geology, 2023a, 157: 106465.

Jiang, H., Wen, L., Zhou, G., et al. Rare earth elements characteristics and diagenetic fluids of dolomites in the Longwangmiao Formation, eastern Sichuan Basin. Natural Gas Geoscience, 2023b, 34: 1187-1202. (in Chinese)

Kawabe, I., Toriumi, T., Ohta, A., et al. Monoisotopic REE abundances in seawater and the origin of seawater tetrad effect. Geochemical Journal, 1998, 32(4): 213-229.

Kovalevych, V. M., Zang, W. L., Peryt, T. M., et al. Deposition and chemical composition of Early Cambrian salt in the eastern Officer Basin, south Australia. Australian Journal of Earth Sciences, 2006, 53(4): 577-593.

Land, L. S. The origin of massive dolomite. Journal of Geological Education, 1985, 33: 112-125.

Liang, J., Liu, S., Li, L., et al. Geochemical constraints on the hydrothermal dolomitization of the middle-upper Cambrian Xixiangchi Formation in the Sichuan Basin, China. Frontiers in Earth Science, 2022, 10: 927066.

Li, C., Liu, K., Liu, J. A petroliferous Ediacaran microbial-dominated carbonate reservoir play in the central Sichuan Basin, China: Characteristics and diagenetic evolution. Precambrian Research, 2023, 384: 106937.

Li, D., Ling, H., Jiang, S., et al. New carbon isotope stratigraphy of the Ediacaran-Cambrian boundary interval from SW China: implications for global correlation. Geological Magazine, 2009, 146(4): 465-484.

Liu, D., Cai, C., Hu, Y., et al. Multistage dolomitization and formation of ultra-deep Lower Cambrian Longwangmiao Formation reservoir in central Sichuan Basin, China. Marine and Petroleum Geology, 2021a, 123: 104752.

Liu, L., Gao, Y., Wang, D., et al. The impact of gypsum salt rock on Cambrian subsalt dolomite reservoir in Tarim Basin. Acta Petrologica et Mineralogica, 2021b, 40(1): 109-120. (in Chinese)

Liu, S., Yang, Y., Deng, B., et al. Tectonic evolution of the Sichuan Basin, Southwest China. Earth-Science Reviews, 2021c, 213: 103470.

Li, X., Zhu, G., Zhang, Z. Genesis of ultra-deep dolostone and controlling factors of large-scale reservoir: A case study of the Sinian Dengying Formation and the Cambrian Longwangmiao Formation in the Sichuan Basin. Science China Earth Sciences, 2024, 67(7): 2352-2382.

Li, Y., Liu, G., Song, Z., et al. Constraints of C–O–Sr isotope and elemental geochemistry on the origin of dolomite of the deeply buried Ediacaran sedimentary succession,

central Sichuan Basin (SW China). Journal of Asian Earth Sciences, 2023, 255(1): 105780.

Li, Y., Xu, W., Fu, M., et al. Dolomitization Controlled by Paleogeomorphology in the Epicontinental Sea Environment: A Case Study of the 5th Sub-Member in 5 Member of the Ordovician Majiagou Formation in Daniudi Gas Field, Ordos Basin. Minerals, 2021, 11(8): 827.

Lottermoser, B. Rare earth elements and hydrothermal ore formation processes. Ore Geology Reviews, 1992, 7(1): 25-41.

Machel, H. G. Concepts and models of dolomitization: A critical reappraisal. Geological Society, London, Special Publications, 2004, 235: 7-63.

Mattes, B. W., Mountjoy, E. W. Burial dolomitization of the Upper Devonian Miette buildup, Jasper National Park, Alberta, in Concepts and Models of Dolomitization, edited by D. H. Zenger, J. B. Dunham and R. L. Ethington, SEPM Special Publication, Texas, pp. 259-297, 1980.

Nothdurft, L. D., Webb, G. E., Kamber, B. S. Rare earth element geochemistry of Late Devonian reefal carbonates, Canning Basin, Western Australia: Confirmation of a seawater REE proxy in ancient limestones. Geochimica et Cosmochimica Acta, 2004, 68, 263-283.

Patterson, R. J., Kinsman, J. J. Formation of diagenetic dolomite in coastal sabkha along Arabian (Persian) Gulf. AAPG Bulletin, 1982, 66(1): 28-43.

Preto, N., Breda, A., Dal Corso, J., et al. Primary dolomite in the late Triassic Travenanzes formation, dolomites, northern Italy: Facies control and possible bacterial influence. Sedimentology, 2015, 62: 697-716.

Qing, H., Mountjoy, E. W. Rare earth element geochemistry of dolomites in the Middle Devonian Presqu'ile barrier, Western Canada Sedimentary Basin: Implications for fluid-rock ratios during dolomitization. Sedimentology, 1994, 41: 787-804.

Qing, H., Veizer, J. Oxygen and carbon isotopic composition of Ordovician brachiopods: Implications for coeval seawater. Geochimica et Cosmochimica Acta, 1994, 58: 4429-4442.

Roberts, J. A. The problem with dolomite. Nature Geoscience, 2024, 17: 716-716.

Ryan, B. H., Kaczmarek, S. E., Rivers, J. M. Early and pervasive dolomitization by near-normal marine fluids: New lessons from an Eocene evaporative setting in Qatar. Sedimentology, 2020, 67: 2917-2944.

Sibley, D. F., Gregg, J. M. Classification of dolomite rock textures. Journal of Sedimentary Research, 1987, 57(6): 967-975.

Song, J., Zhang, Y., Yin, K., et al. Characteristics and geological significance of mixed sediments in the Lower Cambrian Longwangmiao Formation, central Sichuan Basin. Oil & Gas Geology, 2021, 42(3), 627-638. (in Chinese)

Veizer, J., Ala, D., Azmy, K., et al. $^{87}Sr/^{86}Sr$, $\delta^{13}C$ and $\delta^{18}O$ evolution of Phanerozoic seawater. Chemical Geology, 1999, 161: 59-88.

Wang, J., Hu, Z., Hu, J., et al. Controlling factors and reservoir characteristics of Dolostone-evaporite co-occurring systems in the Eastern Sichuan Basin, China. Carbonates and Evaporites, 2023, 38: 82.

Wang, L., Hu, W., Wang, X., et al. Seawater normalized REE patterns of dolomites in Geshan and Panlongdong sections, China: Implications for tracing dolomitization and diagenetic fluids. Marine and Petroleum Geology, 2014, 56: 63-73.

Wang, Y., Shi, Z., Qing, H., et al. Petrological characteristics, geochemical characteristics, and dolomite model of the lower Cambrian Longwangmiao Formation in the periphery of the Sichuan Basin, China. Journal of Petroleum Science and Engineering, 2021, 202: 108432.

Warren, J. Dolomite: Occurrence, evolution and economically important associations. Earth-Science Reviews, 2000, 52(1-3): 1-81.

Warren, J. K. Evaporites through time: Tectonic, climatic and eustatic controls in marine and nonmarine deposits. Earth-Science Reviews, 2010, 98(3-4): 217-268.

Wei, G., Hood, A. V. S., Planavsky, N. J., et al. Calcium isotopic constraints on the transition from Aragonite Seas to Calcite Seas in the Cambrian. Global Biogeochemical Cycles, 2022, 36: e2021GB007235.

Wei, G., Zhu, Y., Zheng, J., et al. Tectonic-lithofacies paleogeography, large-scale source-reservoir distribution and exploration zones of Cambrian subsalt formation, Tarim Basin, NW China. Petroleum Exploration and Development, 2021, 48(6): 1114-1126.

Xiang, P., Ji, H., Shi, Y., et al. Petrographic, rare earth elements and isotope constraints on the dolomite origin of Ordovician Majiagou Formation (Jizhong Depression, North China). Marine and Petroleum Geology, 2020, 117: 104374.

Xu, A., Hu, S., Wang, Z., et al. Sedimentary mode and reservoir distribution of the Cambrian carbonate & evaporate paragenesis system in the Sichuan Basin. Natural Gas Industry B, 2016, 3(5): 418-427.

Yang, W., Li, T., Lan, C., et al. Distribution and controlling factors of dolostone in lower Cambrian Longwangmiao Formation, Sichuan Basin. Earth Science, 2024, 49(7): 2388-2406. (in Chinese)

Zhang, X., Gao, Z., Maselli, V., et al. Tectono-sedimentary characteristics and controlling factors of the lower-middle Cambrian gypsum-salt rocks in the Tarim Basin, Northwest China. Marine and Petroleum Geology, 2023, 151: 106189.

Zhao, Y., Gao, D., Hu, M., et al. Controls of paleoclimate and sea-level changes on the high-frequency sequence of shallow-water carbonates: A case study of the Longwangmiao Formation in the central Sichuan Basin. Geology of China, 2024, 51: 577-591. (in Chinese)

Zhou, J., Xu, C., Yao, G., et al. Genesis and evolution of lower Cambrian Longwangmiao formation reservoirs, Sichuan Basin, SW China. Petroleum Exploration and Development, 2015, 42(2): 175-184.